TPM Vol. 32, No. S9, 2025 ISSN: 1972-6325 https://www.tpmap.org/



EFFICIENT BRAIN TUMOR SEGMENTATION WITH 3D U-NET AND PRETRAINED BACKBONES

ZAHRA FASKA^{1*}, LAHBIB KHRISSI², IMADEDDINE MOUNTASSER³, KHALID HADDOUCH⁴, NABIL EL AKKAD⁵

1.2.3,4,5 DEPARTMENT LABORATORY OF APPLIED SCIENCES AND EMERGING TECHNOLOGIES ENSA, SIDI MOHAMED BEN ABDELLAH UNIVERSITY FEZ, MOROCCO

EMAIL: lahbib.khrissi@usmba.ac.ma²; imountasser@gmail.com³; khalid.haddouch@usmba.ac.ma⁴; nabil.elakkad@usmba.ac.ma⁵

Abstract— Segmentation of a brain tumor from three-dimensional data is one of the very important and very challenging tasks within the scope of medical image analysis since whatever is manual-segmented by human operators may lead to imprecision in diagnosis and treatment. Some new methods have recently been developed for tumor segmentation within magnetic resonance imaging data using two-dimensional and three-dimensional convolutions. However, a 2D convolution does not make full user of the spatial information which comes natural with volumetric study medical imaging data, and 3D convolutions come with much computation overhead and much memory resource. This tries to address that problem by using the 3D U-Net architecture, specifically for brain tumor MRI images. Effects of the use of pre-trained backbone networks into the 3D U-Net model were studied here within three main configurations: the usual 3D U-Net, 3D U-Net with enhancement using ResNet50, and 3D U-Net incorporated with VGG16. The model was tested with actual data obtained from the BraTS2020 datasets. A compare and validate analysis were done. Different metrics like accuracy, Dice Coefficient, cross-entropy loss, precision, sensitivity, and specificity were focused on in the comparison. The accuracies of 3D UNet, 3D-UNet pre-trained with ResNet50 backbone, and 3D-UNet pre-trained with VGG16 backbone were found to be 0.9798, 0.9795, and 0.9810, respectively. Dice Coefficient scores were noted as 0.9993, 0.9976, and 0.9996 in the same order. Therefore, these proposed methods are competitive with state-of-the-art approaches in this specific domain. But better results were found with the model that combines the 3D UNet model with a VGG16 pre-trained backbone for segmentation of brain tumors.

Keywords— Brain tumor segmentation, 3D MRI, 3D U-Net, Pretrained backbone networks, VGG16; resnet50, BraTS dataset

I. INTRODUCTION

Tumors found in the brain signify an overgrowth of abnormal cells that have the potential to harm the nervous system and interfere with surrounding healthy brain tissue. As one of the most vital organs, the human brain manages a multitude of functions within the body. These tumors can significantly impair the overall functionality of the brain and are regarded as some of the most perilous diseases affecting humans [1]. In the year 2022, it is estimated that primary malignant brain tumors in adults accounted for 18,280 fatalities in the United States [2]. The term intracranial tumors encompass all definitions of neoplasms known to arise from the intracranial tissues of the brain, comprising heterogeneous populations of cancer cells emanating from the brain with various degrees of malignancy arising in benign tumors of the brain [3,4]. In addition, automatic medical image segmentation is also extremely critical preparatory steps for analysis medical images as it helps greatly reduce challenges that are typically encountered with laborious and time-consuming manual segmentations. Therefore, high value and importance lie in creating an automatic segmentation algorithm [5–23]. Deep learning approaches [24,25], because by now they have achieved valuable supremacy in robust feature representation and generalization, are being widely applied in many applications related to computer vision and processing medical images, particularly with regard to brain tumor segmentation [26].

In recent years, CNNs have efficient robust generalization and have hence become very popular for medical image segmentation. Earlier works [27, 28] focused on making the network deeper by adding more convolutional and pooling layers in improving the segmentation accuracy, which was not better due to high network layer counting leads to decay; that decay was solved by introducing ResNet [29]. Since the proposal of the U-net architecture [30], it was the most preferred framework used by researchers for medical image segmentation. Several versions with modification in the original U-Net architecture, which in turn increases the improvement of accuracy, were



proposed [31]. As long as the algorithms are developed, the trend moves toward more and more precision. But actual pixels within a large imbalance between healthy and tumoral tissue do not lead to very great accuracy in the segmentation of brain tumors.

The U-Net simply uses concatenation to combine the features and then simply forwards the resulting information to perform classification. Overwhelming majority studies in Brain Tumor Segmentation (BTS) used 2D or 3D convolutions while training deep CNN models. While 2D convolution does not make excellent use of the spatial information available in medical images, 3D convolution is more challenging since it requires a large memory size and high computational power. Most recent state-of-the-art research works on BTS are actually mostly directed towards the further enhancement of already recorded performance in terms of accuracy on the standard BraTS benchmark datasets. Even the most recent cutting-edge segmentation models, including very pronounced U-Net architectures, that could have done this do not have access to 3D volumetric brain tumor scans due to a lack of adequate computational resources. On the flip side, many studies have used 2D slices or images and have taken a patched-based strategy for deep learning model deployment and fine-tuning [32,33,34]. Also, with network depth, the gradient of bottom-up features often becomes diminished to zero, negatively impacting the segmentation results. Up to the most recent, studies apply the U-Net architecture for segmenting MRI images in the detection of brain tumors; though, the U-Net architecture is computationally intensive because of its intricate feature extraction mechanism

The structure of our paper is devised of 5 parts: Sections 2 discusses the methodology and the datasets employed for this study, Section 3 the training and implementation specifics, and Section 4 the experimental results. The last section is where the concluding remarks and future directions are presented.

II. MATERIALS AND METHODS

The primary research method employed in this study is segmentation research, which involves the categorization of brain tumors, alongside comparative research that aims to evaluate the acquired against existing ones to assess the advancements achieved. To facilitate model training, 3D MRI images were required. The data for this paper was taken from the BRATS2020 dataset freely available on the internet and already preprocessed into groups to use it for training and testing.

A. Dataset

Model validation was done using the open BraTS 2020 challenge dataset from MICCAI. This set includes 3D MRI scans of the brains of 369 glioma patients; there were 76 patients with LGG and the rest with HGG. Two images represent each patient and measure 240×240 pixels, and 155 slices compose each 3D scan. Four MRI scans from the modalities T2, T1ce, T1, and FLAIR are available for each subject. This paper shows the subject samples of the benchmark BraTS 2020 dataset having all four modalities and their corresponding truths.

B. Pre-Processing

Variations in the intensities of MRI images can result from discrepancies in the magnetic fields produced by the scanners. Therefore, it is crucial to perform preprocessing steps prior to integrating the images into the training model to improve segmentation outcomes. This process involves standardizing and normalizing each image by subtracting the mean from each voxel and subsequently dividing by the standard deviation. Consequently, every brain image achieves a mean of zero and a unit variance, a technique referred to as Z score normalization [35]. The formula utilized for this normalization procedure is:

$$\mathbf{I_{norm}} = \frac{\mathbf{I} - \mu_i}{\sigma_i} \tag{1}$$

In this context, I and Inorm denote the normalized input and the original images, respectively. The mean value is represented by μ i, while the standard deviation of the input image is indicated as σ i. Due to constraints in memory capacity, all MR images were resized from dimensions of 240x240x155 to 128x128x128. To facilitate the extraction of information from the four sequences, a fusion of all modalities was executed. Consequently, the dimensions of the input training examples were structured as 128x128x128x4, with the numeral 4 representing the four modalities—T1, T1ce, T2, and FLAIR—that were utilized in the model during the training process.

C. Network architecture

Three types of network architecture are considered in this study. The version denoted as 3 UNet serves as our main architecture and it was slightly modified by adding a pretrained backbone networks. Additionally, the same experimental procedure was conducted with 3D UNet, specifically the 3D-UNet that employs ResNet50 as its backbone, as well as the 3D-UNet utilizing VGG16 as its backbone.

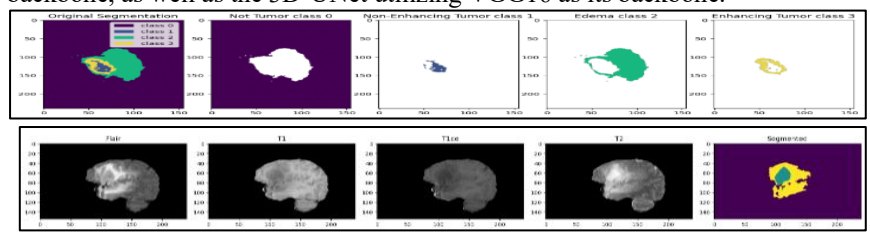


Fig. 1. MRI image samples and their ground truth for all four modalities (class 0: not tumor (NT) representing a healthy area or background; class 1: Necrotic and Non-enhending Tumor (NCR + NET); class 2: peritumoral eDEma (ED); class 3: Enhancing tumor (ET))

ISSN: 1972-6325 https://www.tpmap.org/



a) 3D-Unet network

U-Net is one of the most commonly used architectures for segmentation tasks. It is specifically developed for the segmentation of medical images, among which it proves to be very effective in applications such as cell tracking. When testing with several hundred image samples, the results from U-Net appear to be very favorable most of the time. The architecture of U-Net is a "U" shape that comprises two main parts conveying different roles, one for contraction and the other for expansion. The contraction pathway involves operations of down-sampling and down-convolution, while the expansion pathway incorporates up-sampling and up-convolution. During the contraction phase, the feature maps' spatial dimensions are reduced, whereas, in the expansion phase, these dimensions are restored to their original scale. Although originally developed for 2D images, the model can be adapted for 3D convolutions by substituting 2D convolutional networks with their 3D counterparts. Figure 2 illustrated the architecture of the 3D-Unet network.

b) ResNet-50 as pretrained backbone network

The network ResNet-50 comprises 50 convolutional layers, with pooling and fully connected layers, and it has some more layers of convolution inside residual blocks. The building blocks of this architecture are such that each block aims at approximating some residuals in the function learned; that is, the difference between what the real output of a certain set of convolution layers is and what the current output approximates. By learning this residual function, the network effectively addresses the challenges posed by vanishing gradients. Furthermore, this pretraining enhances the accuracy of the network when it undergoes fine-tuning for a particular task.

c) Vgg16 as pretrained backbone network

The VGG-16 from the family of VGG [36] is very popular backbones not just in computer vision but in various applications of computer science; effectiveness with VGG architectures has been demonstrated in tasks associated with image classification as well as object detection. The year when this paper came out was 2014 and since that point, in time, VGG-16 is typically considered to be the basic deep learning backbone having 16 layers wherein 13 layers are convolutional layers, 5 are max-pooling, and three are fully connected; using the ReLU activation function

III.RESULTS AND DISCUSSIONS

This section provides an in-depth examination of the evaluation metrics utilized to assess the effectiveness of the proposed model, including implementation specifics, the results achieved, and a comparative analysis with current state-of-the-art approaches.

A. Evaluation measure

For the experiment, the following evaluation metrics are used:

• Categorical cross-entropy loss: the loss is calculated using categorical cross-entropy [37]. It quantifies the divergence between the two probability distributions. How much the predicted class is or is not the actual class of the object is indicated by this value of loss. It calculates the loss function of categorical cross-entropy as follows:

$$loss = \sum_{i=1}^{\text{output size}} \mathbf{Ai. log} \hat{\mathbf{A}} i$$
 (2)

In this context, $\widehat{\mathbf{A}}$ i gives the i-th scalar value of the model output, Ai gives its corresponding target value, and the output size is the total count of scalar values in the model output.

• Similarity index of Dice coefficient [38]: This metric quantifies the overlap area between the two images; if A represents the area delineated by the segmentation algorithm and B denotes the area defined by the ground truth, the measure D can be articulated as:

$$D(A, B) = \frac{2|A \cap B|}{|A| + |B|} \tag{3}$$

• Accuracy: One of the criteria we use to evaluate our classification models is Accuracy. Precision can be easily validated using the confusion matrix applying the theorem outlined below.

Accuracy =
$$\frac{\text{TP+TN}}{\text{TP+TN+FP+FN}}$$
 (3)

• Precision: is defined as the ratio of true positives to their sum with false negatives.

$$precision = \frac{TP}{TP + FP}$$
 (4)

• Sensitivity: The ratio of true positive pixels to the count of all pixels correctly predicted. The equation for calculating sensitivity is presented in Eq (5).

$$Sensitivity = \frac{TP}{TP+FN}$$
 (5)

• Specificity: is the ratio of accurately identified true negative pixels and plays a major role in determining whether or not tumor regions have been either over- or under-segmented.



ISSN: 1972-6325 https://www.tpmap.org/

TPM Vol. 32, No. S9, 2025

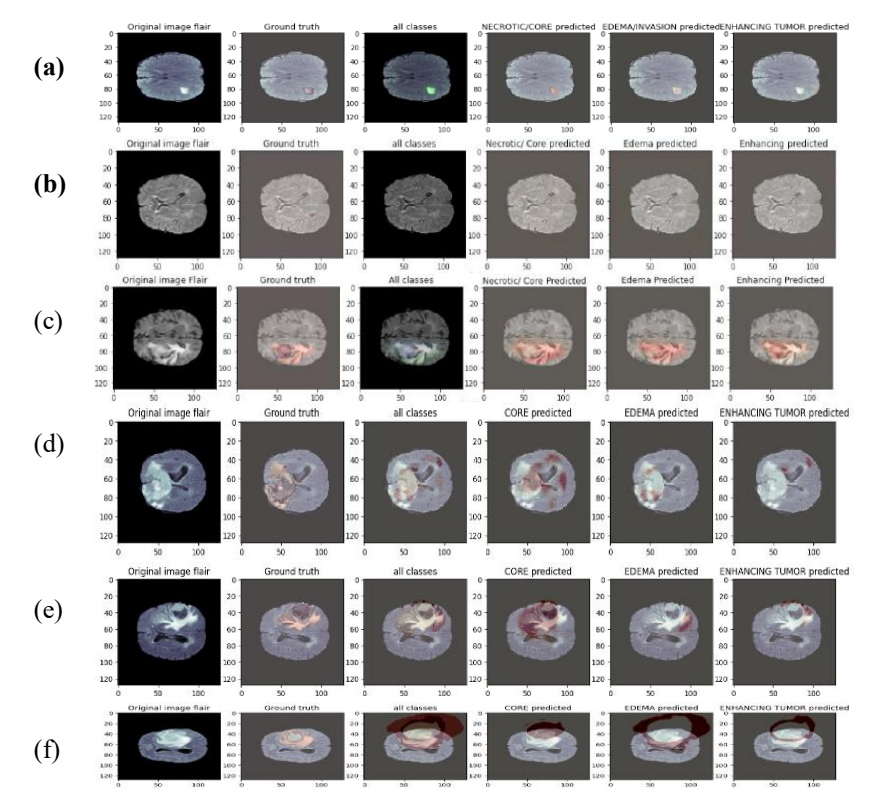
 $Specificity = \frac{TN}{TN+FP}$ (6)

B. Implementation detail

The 3D U-Net was implemented through the Python programming language, with Keras and TensorFlow providing the necessary frameworks. In this setup, the experiments utilized the ADAM optimizer, which functioned at a learning rate of 0.0001. The model incorporated the ReLU activation function in conjunction with batch normalization, a method that generally stabilizes the model and normalizes each layer within the network. Due to constraints in computational resources, the model training was limited to 30 epochs, employing a batch size of 3. Experiments were performed using the BraTS 2020 benchmark dataset, with 80% of the data designated for training, 10% for testing, and the remaining 10% for validation. Training occurred on a Tesla T4 GPU with 25 GB of RAM, accessed through Google Colab Pro. A range of experiments was conducted to identify the optimal hyperparameter set for the proposed networks.

A. Analysis of the results

In this study, a comparison was conducted between 3D UNet, 3D-UNet with a Resnet50 backbone, and 3D-UNet utilizing a vgg16 backbone to generate a 3D volume of the segmentation mask that delineates the tumor regions WT, ET, and TC. The results of the MRI images in the axial plane are qualitatively illustrated in Fig. 2, featuring randomly selected slices. The predictions presented below were derived from Random Images to demonstrate the algorithm's predictive accuracy. As evidenced in Fig. 2, which depicts images of a brain with a tumor, our predictions align closely with the ground truth. The evaluation of the models involved generating various metrics using the test data, which are presented in Table 1 below—these metrics include accuracy, loss, dice coefficient, precision, sensitivity, and specificity. The saved model was employed to conduct evaluations based on the specified metrics, resulting in a scorecard that displays these metrics for both the training set and the validation set. The 3D UNet model attained accuracy and Dice Coefficients of 0.9798 and 0.9993, respectively.



Models	3D UNet		3D-UNet with a Resnet50 backbone		3D-UNet with a vgg16 backbone	
Metric	Training Score	Validation Score	Training Score	Validation Score	Training Score	Validation Score
Accuracy	0.9855	0.9798	98.54	0.9795	0.9859	0.9810
Loss	0.8040	0.8230	0.8041	0.8264	0.7992	0.8080
Dice Coefficient	0.9992	0.9993	0.9975	0.9976	0.9995	0.9996
Precision	0.9860	0.9804	0.9861	0.9802	0.9863	0.9814
Sensitivity	0.9852	0.9795	0.9850	0.9791	0.9857	0.9808
Specificity	0.9953	0.9935	0.9954	0.9934	0.9954	0.9938



Fig. 2. Prediction using existing models: (a) Unet, (b) ResNet-50, (c) VGG-16, (d) 3D Unet, (e) 3D-UNet with backbone ResNet-50 pretrained, and (f) 3D-UNet with Vgg16 pretrained backbone

The figure demonstrates that visual analysis reveals a close correspondence between the predictions and the ground truth, particularly when compared to the 3D-UNet model utilizing a Resnet50 pretrained backbone, which achieved accuracy and Dice Coefficients of 0.9795 and 0.9976, respectively. This model exhibited a decline of 0.12% in accuracy and 0.17% in the Dice Coefficient relative to the conventional 3D-UNet. Conversely, the 3D-UNet model employing a Vgg16 pretrained backbone recorded accuracy and Dice Coefficients of 0.9810 and 0.9996, respectively. The findings for the 3D-UNet with a Vgg16 pretrained backbone indicated an enhancement of 0.88% in the Dice Coefficient and a slight increase of 0.03% in accuracy compared to the standard 3D-UNet. A quantitative summary of all architectures is provided in Table 2, detailing the results for the training, validation, and testing sets. According to the data presented in this table, the 3D-UNet with a Vgg16 pretrained backbone emerged as the superior model among all evaluated, based on metrics such as accuracy, Dice Coefficient, Precision, Sensitivity, and Specificity. The graphs depicting accuracy, Dice Coefficient, and loss are illustrated in the figures. To evaluate the performance of the U-Net architecture in comparison to other leading techniques for brain tumor segmentation, a comparative study must be conducted. This investigation will utilize the same dataset to assess the metrics of various algorithms. Figure 2 displays the visualized images produced by four existing methods, which include standard implementations of 2D U-Net, VGG-16, and ResNet-50. From the subjective evaluation, it appears that the 3D U-Net model utilizing a VGG16 pretrained backbone outperforms the alternatives. The subsequent table, referred to as Table 2, presents quantitative data regarding the performance of the proposed 3D U-Net models in relation to state-of-the-art methods within the tumor core and enhancing tumor categories. Notably, the 3D U-Net with a VGG16 pretrained backbone yielded commendable results for the whole tumor, achieving performance levels comparable to the leading methods available. In summary, this approach appears to provide a more effective means of generating images that are accurately labeled as ground truth.

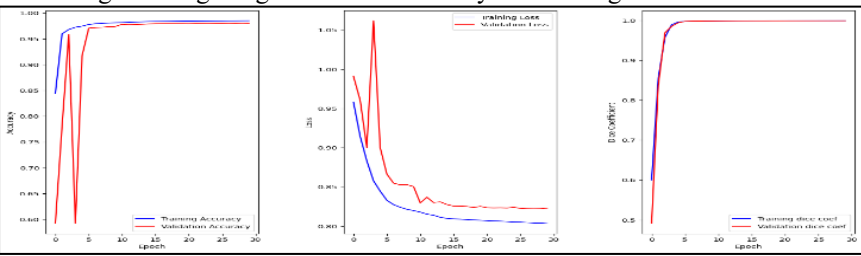


Fig. 3. 3D UNet evaluation graphs.

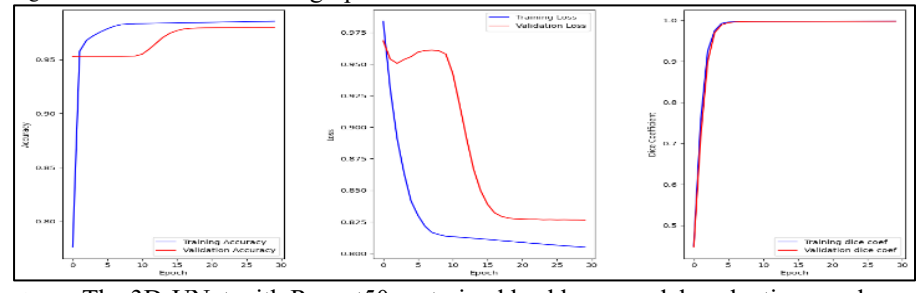


Fig. 4. The 3D-UNet with Resnet50 pretrained backbone model evaluation graphs.

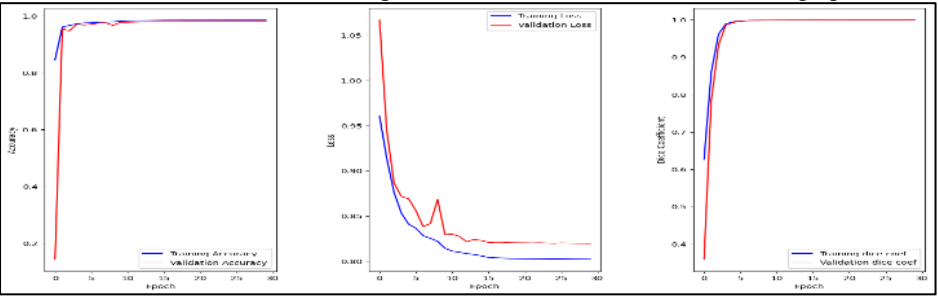


Fig. 5. The 3D-UNet with Vgg16 pretrained backbone model evaluation graphs TABLE II. THE COMPARISON OF ACHIEVED 3DU-NET MODELS WITH EXISTING BTS TECHNIQUES ON THE BENCHMARKS BRATS 2020 DATASET.

Paper	Network	Image Dimension	Dice Score (WT)
[39]	'TransBTS'	128 × 128 × 128	0.9009
[40]	'3D U-Net'	128 × 128 × 128	0.8411
[41]	'2D Deep Residual U-Net'	2D Slices with 240×240	0.8673



ISSN: 1972-6325 https://www.tpmap.org/

TPM Vol. 32, No. S9, 2025

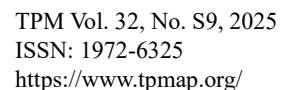
[42]	'Modified 3D U-Net by embedding and re-using any 2D classifier network'	192 × 160 × 108	0.8068
[43]	'3D encoder-decoder based V-Net model'	64 × 64 × 64	0.8463
[44]	'Lightweight decoder and heavy encoder based modified 3D U-Net with residual and dense blocks'	128 × 128 × 128	0.90
[44]	'DResU-Net'	128 × 128 × 128	0.8660
ours	The 3D-UNet using Resnet50 pretrained backbone The 3D-UNet using Vgg16 pretrained backbone	128 × 128 × 128	0.9976 0.9996

IV.CONCLUSIONS

This study focuses on the challenge of segmenting brain tumors within three-dimensional MRI images. To improve the efficacy of tumor segmentation from MRI scans, a 3D Deep U-Net architecture is proposed. The research examines the influence of the 3D U-Net both with and without pretrained backbone networks. Specifically, three configurations are analyzed: the standard 3D-UNet, the 3D-UNet utilizing a ResNet50 pretrained backbone, and the 3D-UNet employing a VGG16 pretrained backbone. The proposed models underwent evaluation using the BraTS 2020 benchmark dataset. The experimental findings indicate that the 3D-UNet incorporating the VGG16 pretrained backbone outperformed the other configurations, achieving a 0.88% increase in the Dice Coefficient and a 0.03% rise in accuracy relative to the standard 3D-UNet, thus reflecting improved segmentation precision. The 3D-UNet model with a pretrained backbone yielded promising results in this investigation. Future research aimed at further enhancing model performance could concentrate on optimizing fine-tuning methods, applying dataset augmentation strategies, and conducting comprehensive post-processing. Quantitative assessments demonstrated that our models attain state-of-the-art methods accuracy on established MRI dataset.

REFERENCES

- [1] Z. Liu et al., "Deep Learning Based Brain Tumor Segmentation: A Survey," 14(8), pp. 1–21, 2020, [Online]. Available: http://arxiv.org/abs/2007.09479.
- [2] A. Tahir, M. Asif, M. Bin Ahmad, T. Mahmood, M.A. Khan, M. Ali, Brain tumor detection using decision-based fusion empowered with fuzzy logic, Math. Probl Eng. 2022 (Aug. 2022) 1–13, https://doi.org/10.1155/2022/2710285.
- [3] K.D. Miller, et al., Brain and other central nervous system tumor statistics, CA A Cancer J. Clin. 71 (5) (Sep. 2021) 381–406, https://doi.org/10.3322/ CAAC.21693, 2021.
- [4] J.B. Iorgulescu, et al., Molecular Biomarker-Defined Brain Tumors: Epidemiology, Validity, and Completeness in the United States, Neuro Oncol, 2022, https://doi.org/10.1093/NEUONC/NOAC113. Apr.
- [5] L. Khrissi, N. El Akkad, H. Satori, and K. Satori, "Clustering method and sine cosine algorithm for image segmentation," Evol. Intell., 15, 669–682 (2022), doi: 10.1007/s12065-020-00544-z.
- [6] Faska, Z., Khrissi, L., Haddouch, K. et al. A robust and consistent stack generalized ensemble-learning framework for image segmentation. J. Eng. Appl. Sci. 70, 74 (2023).
- [7] L. Khrissi, N. El Akkad, H. Satori, and K. Satori, A Feature Selection Approach Based on Archimedes' Optimization Algorithm for Optimal Data Classification. International Journal of Interactive Multimedia and Artificial Intelligence (IJIMAI), 2023. DOI: https://doi.org/10.9781/ijimai.2023.01.005.
- [8] Khrissi, L., El Akkad, N., Satori, H., & Satori, K.
- (2022). "APerformant Clustering Approach Based on An Improved Sine Cosine Algorithm". International Journ al of Computing, 21(2), 159168. https://doi.org/10.47839/ijc.21.2.2584.
- [9] MOUSSAOUI, Hanae, EL AKKAD, Nabil, et BENSLIMANE, Mohamed. A Brain Tumor Segmentation and Detection Technique Based on Birch and Marker Watershed. SN Computer Science, 2023, vol. 4, no 4, p. 339.
- [10] L. Khrissi, H. Satori, K. Satori, and N. El Akkad, "An Efficient Image Clustering Technique based on Fuzzy C-means and Cuckoo Search Algorithm," Int.
- [11] J. Adv. Comput. Sci. Appl., vol. 12, no. 6, pp. 423432, 2021, doi: 10.14569/IJACSA.2021.0120647.
- [12] MOUSSAOUI, Hanae, EL AKKAD, Nabil, et BENSLIMANE, Mohamed. A hybrid skin lesions segmentation approach based on image processing methods. Statistics, Optimization & Information Computing, 2023, vol. 11, no 1, p. 95-105.
- [13] Khrissi, L., Akkad, N.E.L., Satori, H., Satori, K.. Simple and Efficient Clustering Approach Based on Cuckoo Search Algorithm. 4th International Conference on Intelligent Computing in Data Sciences, ICDS 2020, 2020, 9268754.





- [14] FASKA, Zahra, KHRISSI, Lahbib, HADDOUCH, Khalid, et al. Random Forest for Semantic Segmentation Using Pre-Trained CNN (VGG16) Features. In: Digital Technologies and Applications: Proceedings of ICDTA'23, Fez, Morocco, Volume 2. Cham: Springer Nature Switzerland, 2023. p. 510-520.
- [15] Khrissi, L., Akkad, N.E., Satori, H., Satori, K. Color image segmentation based on hybridization between Canny and k-means. 7th Mediterranean Congress of Telecommunications 2019, CMT 2019, 2019, 8931358.
- [16] Z. Faska, L. Khrissi, K. Haddouch and N. El Akkad, "Seg_UResNet: A Deep Hybrid Convolutional Neural Network of Road Scenes for semantic segmentation," 2024 International Conference on Circuit, Systems and Communication (ICCSC), Fes, Morocco, 2024, pp. 1-8, doi: 10.1109/ICCSC62074.2024.10616428.
- [17] Moussaoui H, Benslimane M, El Akkad N (2022) Image segmentation approach based on hybridization between K-means and Mask R-CNN. In: WITS 2020. Springer, Singapore, pp 821–830.
- [18] Faska Z, Khrissi L, Haddouch K, El Akkad N (2021) A powerful and efficient method of image segmentation based on random forest algorithm. In: International Conference on Digital Technologies and Applications. Springer, Cham, pp 893–903 8.
- [19] L. Khrissi, Nabil El Akkad, Hassan Satori, Khalid Satori. A Feature Selection Approach Based on Archimedes' Optimization Algorithm for Optimal Data Classification. IJIMAI, 2023. DOI: https://doi.org/10.9781/ijimai.2023.01.005
- [20] H. Moussaoui, N. El Akkad, M. Benslimane, W. El-Shafai, A. Baihan, Ch. Hewage, R. Singh Rathore. Enhancing automated vehicle identification by integrating YOLO v8 and OCR techniques for high-precision license plate detection and recognition. Scientific Reports, 2024, 14(1), 14389.
- [21] Touil, H., El Akkad, N., Satori, K. H-rotation: Secure storage and retrieval of passphrases on the authentication process. International Journal of Safety and Security Engineering, 2021, 10(6), pp. 785–796
- [22] Boudine, B., Kramm, S., Akkad, N.E., ... Saaidi, A., Satori, K. A flexible technique based on fundamental matrix for camera self-calibration with variable intrinsic parameters from two views. Journal of Visual Communication and Image Representation, 2016, 39, pp. 40–50
- [23] Es-sabry, M., El Akkad, N., Satori, S., El-Shafai, W., Torki, T., Rajkumar, S., An efficient 32-bit color image encryption technique using multiple chaotic maps and advanced ciphers. Egyptian Informatics Journal, 2024, 25, 100449
- [24] Moussaoui, H., Akkad, N.E., Benslimane, M., Walid, E., Abdullah, B., Chaminda, H. & Rajkumar Singh, R.. Scientific Reports, 2024, 14(1), 14389
- [25] Y. Wang, G. Zhao, K. Xiong, G. Shi, Msff-net: multi-scale feature fusing net-works with dilated mixed convolution and cascaded parallel framework for sound event detection, Digit. Signal Process. 122 (2022) 103319. [26] A. Khodadadi, S. Molaei, M. Teimouri, H. Zare, Classification of audio codecs with variable bit-rates using deep-learning methods, Digit. Signal Process. 110 (2021) 102952.
- [27] M.I. Razzak, M. Imran, G. Xu, Efficient brain tumor segmentation with multi-scale two-pathway-group conventional neural networks, IEEE J. Biomed. Health Inform. 23(5) (2018) 1911–1919.
- [28] Fu, J., Singhrao, K., Zhong, X., Gao, Y., Qi, S. X., Yang, Y., ... Lewis, J. H. (2021). An automatic deep learning—based workflow for glioblastoma survival prediction using preoperative multimodal MR images: A feasibility study. Advances in Radiation Oncology, 6(5), Article 100746. https://doi.org/10.1016/j.adro.2021.100746
- [29] Huang, Z., Zhao, Y., Liu, Y., & Song, G. (2021). GCAUNet: A group cross-channel attention resi-dual UNet for slice based brain tumor segmentation. Biomedical Signal Processing and Control, 70, Article 102958. https://doi.org/10.1016/j. bspc.2021.102958
- [30] Ronneberger, O., Fischer, P., & Brox, T. (2015, October). U-net: Convolutional networks for bi-omedical image segmentation. In International Conference on Medical image computing and computer-assisted intervention (pp. 234-241). Springer, Cham. 10.1007/978-3-319-24574-4 28.
- [31] Tulsani, A., Kumar, P., & Pathan, S. (2021). Automated segmentation of optic disc and optic c-up for glaucoma assessment using improved UNET++ architecture. Biocybernetics and Biomedical Engineering, 41(2), 819–832. https://doi.org/10.1016/j.bbe.2021.05.011.
- [32] M. Havaei, A. Davy, D. Warde-Farley, A. Biard, A. Courville, Y. Bengio, C. Pal, P.- M. Jodoin, H. Larochelle, Brain tumor segmentation with Deep Neural Networks, Med. Image Anal. 35 (2017) 18–31.
- [33] M.I. Razzak, M. Imran, G. Xu, Efficient Brain Tumor Segmentation with Multiscale Two-Pathway-Group Conventional Neural Networks, IEEE J. Biomed. Heal. Informatics 23 (5) (2019) 1911–1919, https://doi.org/10.1109/ JBHI.2018.2874033.
- [34] M. Yaqub, J. Feng, M. Zia, K. Arshid, K. Jia, Z. Rehman, A. Mehmood, State-of-the-art CNN optimizer for brain tumor segmentation in magnetic resonance images, Brain Sci. 10 (7) (2020) 1–19, https://doi.org/10.3390/brainsci10070427.
- [35] E.-E. Mohd. Azhari, M.M. Mohd. Hatta, Z. Zaw Htike, S. Lei Win, Tumor detection in medical imaging: a Survey, Int. J. Adv. Inf. Technol. 4 (1) (2014) 21–30, https://doi.org/10.5121/ijait.2013.4103
- [36] Chen, W., Liu, B., Peng, S., Sun, J., Qiao, X. (2019). S3D-UNet: Separable 3D U-Net for Brain Tumor Segmentation. In: Crimi, A., Bakas, S., Kuijf, H., Keyvan, F., Reyes, M., van Walsum, T. (eds) Brainlesion: Glioma, Multiple Sclerosis, Stroke and Traumatic Brain Injuries. BrainLes 2018. Lecture Notes in Computer Science(.), vol 11384. Springer, Cham. doi:10.1007/978-3-030-11726-9_32.
- [37] K. Simonyan, A. Zisserman, Very deep convolutional networks for large-scale image recognition, 2014, arXiv:1409.1556 [cs]

TPM Vol. 32, No. S9, 2025 ISSN: 1972-6325 https://www.tpmap.org/



- [38] Rusiecki A. Trimmed categorical cross-entropy for deep learning with label noise. Electron Lett. 2019;55. https://doi.org/10.1049/el.2018.7980.
- [39] Dice LR. Measures of the amount of ecologic association between species. Ecology. 1945;26(3):297–302.
- [40] W. Wang, C. Chen, M. Ding, H. Yu, S. Zha, J. Li, TransBTS: multimodal brain tumor segmentation using transformer, Lect. Notes Comput. Sci. (including Subser. Lect. Notes Artif. Intell. Lect. Notes Bioinformatics) vol. 12901 LNCS (2021) 109–119, https://doi.org/10.1007/978-3-030-87193-2_11.
- [41] O. Çiçek, A. Abdulkadir, S.S. Lienkamp, T. Brox, O. Ronneberger, 3D U-net: Learning dense volumetric segmentation from sparse annotation, Lect. Notes Comput. Sci. (including Subser. Lect. Notes Artif. Intell. Lect. Notes Bioinformatics) vol. 9901 LNCS (2016) 424–432, https://doi.org/10.1007/978-3-319-46723-8 49.
- [42] J. Colman, L. Zhang, W. Duan, and X. Ye, "DR-Unet104 for Multimodal MRI Brain Tumor Segmentation," Lect. Notes Comput. Sci. (including Subser. Lect. Notes Artif. Intell. Lect. Notes Bioinformatics), vol. 12659 LNCS, no. 2021, pp. 410–419, 2021, doi: 10.1007/978-3-030-72087-2_36.
- [43] H. Messaoudi, et al., Efficient Embedding Network for 3D Brain Tumor Segmentation, Lect. Notes Comput. Sci. (including Subser. Lect. Notes Artif. Intell. Lect. Notes Bioinformatics) vol. 12658 LNCS (2021) 252–262, https://doi.org/10.1007/978-3-030-72084-1_23
- [44] L. M. Ballestar and V. Vilaplana, "Brain Tumor Segmentation using 3D-CNNs with Uncertainty Estimation," pp. 1–11, 2020, [Online]. Available: http://arxiv.org/abs/2009.12188.
- [45] Raza, Rehan and Bajwa, Usama Ijaz and Mehmood, Yasar and Anwar, Muhammad Waqas and Jamal, Muhammad Hassan, DResU-Net: 3D Deep Residual U-Net Based Brain Tumor Segmentation from Multimodal MRI. Available at SSRN: https://ssrn.com/abstract=4024177 http://dx.doi.org/10.2139/ssrn.4024177.